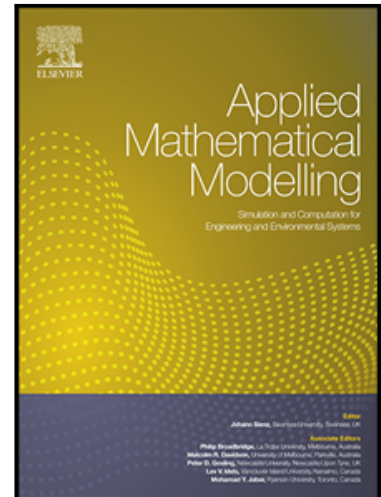# Journal Pre-proof

Analysis and verification of cable pretension effect on the buckling load of a single-link flexible mechanism

Lewei Tang , Marc Gouttefarde , Alberto Doria , Haining Sun , Hongbing Wang , Changjiang Zhou

Highlights

- Dynamic model of a single-link system with pretensioned cables is developed.
- Effect of cable pretension is investigated through von Kármán nonlinearity.
- Analytical formulation of buckling load is derived from dynamical modelling.
- Results from ANSYS buckling analysis are compared with calculated results.
- Experimental verification of link buckling with cable pretension is performed.

Analysis and verification of cable pretension effect on the buckling load of a single-link flexible mechanism

Lewei Tang[1,*], Marc Gouttefarde[2], Alberto Doria[3], Haining Sun[4], Hongbing Wang[1], Changjiang Zhou[1,*]

1. College of Mechanical & Vehicle Engineering, Hunan University, Changsha, 410082, China

2. LIRMM , Univ Montpellier, CNRS, Montpellier, 34095, France

3. Department of Industrial Engineering, University of Padova, Padova, 35131, Italy

4. Department of Mechanical Engineering, Tsinghua University, Beijing, 100084, China

Abstract

This paper utilizes the extended Hamilton's principle to develop a dynamic model of a single-link flexible mechanism with two cables involving the cable pretensions. The effect of cable pretension is considered by introducing the von Kármán nonlinearity into the dynamical modelling. Before implementing the modal analysis, buckling of the flexible beam is investigated with the goal of analyzing structural stability for the single-link flexible system with two pre-tensioned cables. Based on the proposed dynamical model, a transcendental equation for determining the critical buckling load on the beam is derived. Several typical cable and beam materials are included to investigate their influence on the buckling load. An alternative approach to predict the buckling load for the flexible beam braced by cables is applied using the concept of lateral stiffness at the tip, which leads to the same stability equation as that from the presented dynamical model. Finite element simulations are accomplished in ANSYS. The buckling loads obtained from ANSYS are compared with the analytical values based on the proposed method, which demonstrates the effectiveness of the modelling. In addition, an approximate procedure for estimating the critical buckling load is also performed in ANSYS on the basis of a linear relationship between lateral stiffness and buckling load. Finally, an experimental testbench is built and the buckling phenomenon is identified with increasing cable pretensions.

Keywords: Single-link flexible mechanism; Buckling load; Cable pretension; Hamilton's principle; Lateral stiffness

Nomenclature

J_m	Moment of inertia of the motor
θ	Angular displacement of the motor
τ	Torque applied by the motor
EI	Bending stiffness of the flexible link
L	Length of the flexible link
ρ	Density per unit length
m_p	Payload mass
J_p	Moment of inertia of the payload
D	Length of the rigid link
$\mathbf{r_{rl}}$	Rigid displacement vector of a curvilinear point on the flexible link in the global inertia frame
s	Location of a point on the flexible link
$v(s,t)$	Transversal deflection of a point s on the flexible link
V_L, V_C	Potential energy of the flexible Euler-Bernoulli beam and of the cable, respectively
F	Axial force from cable pretensions
k	Spring coefficient of the cables
T_{pre}	Cable pretension at the initial position
$\tau_{ac,i}$	Additional tension in the i-th cable
ΔL	Change in the cable length
L_{free}	Free length of cables
$V(s,t)$	Total potential energy of the single-link flexible mechanism with two cables
T_L, T_P	Kinetic energy of the flexible link and the tip mass payload
T	Total kinetic energy of the single-link flexible mechanism with cables
$\delta T, \delta V$	Variation of kinetic energy and potential energy
δW	Variation of virtual work exerted by the rotational motor torque
$\Psi(s)$	Expression only related to the location of a point s
ω	Natural frequency of the flexible link with pretensioned cables
C_i	Constant related to $\Psi(s)$
λ	$= D^2/(D^2 + L^2)$
D^*	$= D/L$
$E_c A_c$	Axial stiffness of the cables
L_c	Length of the cables
χ	$= EI/(E_c A_c L^2)$
k_l	Lateral stiffness of a flexible beam
k_{ls}	Lateral stiffness of the beam and the cables

1. Introduction

Flexible beams have been widely used in the fields of civil engineering and mechanical engineering. For example, many arches and vaults in Italy used metallic beams to release transverse forces of ancient buildings. Besides, as the main components of compliant manipulators, flexible beams are employed in the design of sensors and positioning motion stages. Compliance analysis is performed using an energy-based Maxwell-Mohr method under the small deformation assumption [1]. Song proposed a vibration control approach for a high-rise building as a flexible beam and its capability is proved by experiments [2]. A rigid-flexible manipulator is analyzed using Hamilton's principle and a model-based boundary control method is proposed to suppress vibrations [3]. Several references deal with the determination of the value of the axial force and the unknown boundary conditions of both flexible beams and cables [4-10]. Li proposed a highly accurate frequency-based method for determining the tension of inclined cables during the construction and service stages of cable-stayed bridges [8]. Another vibration-based estimation of axial forces is proposed in [9], which utilizes several sensors to evaluate the axial force and stiffness at the ends of a beam. Moreover, an identification technique is developed in [10] to assess the tensile force of rods in ancient buildings by measuring natural frequencies. In [11], environmental temperature is involved in the cable tension estimation based on frequency presented. Furthermore, measurement uncertainty is accounted for in the estimation of axial force and boundary conditions with the use of interval analysis in [12]. In these studies, the external force applied to the flexible beam is along the central axis of the beam, which is valid for the application of the beam/rod in civil buildings because of its symmetry. As a matter of fact, in other applications such as truss structures, the external force exerted on the flexible beam may not always act along the central axis. In our previous study [13], a single-link flexible mechanism with two cables was proposed to achieve high-speed movement with a lightweight structure. The dynamic modelling without pretension in cables is derived from energy analysis using the classic extended Hamilton's principle. Besides, the mixed variational formulation of slender beams is widely employed to analyze the dynamic properties of geometrically nonlinear composite beams [14,15,16].

Cables can be utilized to improve the stiffness of flexible link systems [13,17,18]. The cable modes of vibration and their interaction with the end-effector are investigated with the dynamic stiffness matrix method in [18,20], especially when non-negligible cable mass and elasticity is considered (e.g., [21]). Besides, a global mode analysis method is proposed to investigate the dynamic modelling of a flexible-link system with a tip mass and a flexible joint [22]. For a cable-stayed beam, it is found in [23] that the cable-deck interaction exerts no influence on the low-order out-of-plane modal frequencies, which shows the effect of the flexible stiffness of the cable-stayed beam on the natural frequency of the cables. However, only a theoretical deduction is provided without experimental verification. A localization factor is introduced to determine the local modes of a simple cable-stayed beam model in [24]. The coupling interaction between the cables and the beam is well-established in the dynamic solutions without considering the effect of cable pretension on the beam. Vibration of a flexible crane cable is suppressed in two-dimensional space using boundary control strategy in [25]. In the present paper, the dynamics of the cables are neglected due to the very low mass of the cables used, while the force at the end of the flexible link, which is due to the variation of cable lengths, will be taken into account. It is worth noting that only one cable is active in suppressing the vibration of the link through cable tension under the assumption that no pretension is added to the two cables [13]. In this situation, the external force (*i.e.*, the force applied by the cables on the beam) is actually not acting along the central axis of the flexible beam. Even though cable pretension is considered, the direction of the net force applied by the two cables at the end of the flexible link will change during the motion. Therefore, the axial force assumption made in the methods proposed in the literature cannot be directly applied to investigate the dynamic characteristics of the flexible single-link system with cables.

The pretension of cables has been taken into consideration in the literature, especially in the field of cable-stayed bridges [26-29]. The design of cross-ties in the cable-stayed bridges have received a particular attention. Numerical simulations and in-situ measurement records have demonstrated the validity of cross-tie configuration systems in mitigating oscillations [26]. It has also been concluded that the performance of the cable network primarily relies on both the geometric properties of the cross-ties and their relative position on two stays of the bridge. One of the most important steps in the process of designing the cross-ties for cable network systems is to define the amount of cable pretension needed to avoid slacking [27]. Several models were used to simulate cable pretension in cable-stayed bridges such as the nonlinear power-law model in [28]. It was used to represent the incipient failure of cables due to snapping or slackening which has been observed in the literature (e.g., [29]).

In the present study, a linear elastic model is adopted for the cables, where a pretension is active only when the cable is in tension (denoted as a unilateral feature in [27]). Generally, cable pretension is maintained to increase the stiffness of the flexible link system. However, bulking effect of the flexible beam should be carefully considered when high cable pretension is used because of structural instability. The maximum cable pretension is limited by the critical bearing capacity of a rod or beam with respect to buckling. The exact solutions to buckling study of rods with various boundary conditions are investigated in [30,31]. Experimental research of simple supported thin-walled columns was presented with the aim of evaluating critical forces in [32]. To improve the measuring accuracy, a testing procedure was proposed through the correction of the lateral load to avoid plastic deformation [33]. In addition, a non-destructive method of predicting the critical buckling force of thin-walled columns was investigated in [34] based on the fundamental frequency. Another study on the experimental determination of buckling load of beams with various end connections was conducted in [35]. Furthermore, critical buckling loading for beams or columns with initial cracks is studied in the literature [36,37]. In practice, the existence of cracks is prevalent for structural components in engineering and causes a lower buckling load than designed critical values [38]. Nevertheless, the present paper will concentrate on the analysis of intact beams and cables used in a flexible mechanism.

On one hand, the issue of the buckling load determination for flexible beams with various boundary conditions has been resolved and experimentally validated in the literature. Usually, an external load is applied on one end of a beam, which leads to the occurrence of buckling phenomenon once the load exceeds the critical buckling load. Regarding the single-link flexible mechanism in our previous work, the addition of two cables has been verified to improve the performance of the system in terms of natural frequency [13]. On the other hand, the cable pretension will affect the complexity of the critical buckling load determination in the cable-stiffened flexible beam considered in the present paper. Cables play a crucial part in both forming a cable-beam structure and exerting pretensions on the beam. To avoid the buckling effect, it is fundamental to estimate the maximum cable pretension for achieving an admissible mechanism motion accuracy. Therefore, the main contribution of this paper is to develop a method that can predict the buckling load for a single-link flexible mechanism with two pretensioned cables. By employing von Kármán nonlinearity due to the cable pretension, a transcendental equation for solving the buckling load is obtained from the dynamical modelling using the extended Hamilton's principle. Moreover, the identical equation is obtained by identifying the structural instability occurring when the lateral stiffness reduces to zero. To further validate the proposed method, a simulation model in ANSYS is built and the resulting buckling loads turn out to be in good agreement with those obtained with the proposed method. More importantly, the analytical and simulation results are both verified by practical experiments on a physical testbed consisting of one flexible beam and two cables.

This paper studies a single-link flexible mechanism with cables for designing a lightweight industrial manipulator with admissible accuracy [13,39]. Other potential applications of the flexible mechanisms with pretensioned cables include suppressing the vibration of satellite solar panels [17] in aerospace, flexible wings [3,40,41] in the field of bio-inspired design and cable-driven rehabilitation devices [42-45] as well as multilink cable-driven manipulators [46].

The following of this paper is organized as follows. The governing equations of motion are obtained as partial differential equations by the Hamilton's principle in Sect. 2. Critical cable pretension yielding beam buckling is investigated on the basis of this dynamic modelling in Sect. 3. Lateral stiffness of the single flexible beam with two cables is deduced in Sect. 4. Simulation of a single-link flexible mechanism is implemented both with and without cables, and the results are discussed in Sect. 5. The testbed is set up and experimental verification is implemented in Sect. 6 while Sect.7 concludes the paper.

2. Dynamic modelling considering cable pre-tension

A single-link flexible mechanism includes a rotational motor, a flexible link, a lightweight rigid link and a tip payload as well as two pretensioned cables as described in Fig.1. The detailed kinematics model of this mechanism is described in previous research [13], which is introduced briefly here for the sake of completeness. J_{m}, θ and τ are three parameters of the rotational motor, which denote the moment of inertia, the angular displacement (positive in anticlockwise direction) and the applied torque. The flexible link is assumed to have a uniform cross-section with bending stiffness EI as well as a length L with density per unit length ρ. The tip mass with inertial properties, namely payload mass m_{p} and moment of inertia J_{p}, is added to study the effect of a grasped object and consequently is attached to the distal end of the flexible link. Due to the nearly small deformation along the z-axis direction (i.e., the direction of gravity) of the global frame, the bending deformation in the x-y plane is only considered in Fig. 1. Each cable is connected to the tip mass and to the distal end of the rigid link with a length equal to $2D$. The global inertial frame of the single-link flexible mechanism is referred to as $o - xy$ frame, and the relative frame $o - x'y'$ is defined with the x' axis along the neutral axis of the undeformed link. The magnitudes of the two cable pretensions are denoted as t_1 and t_2.
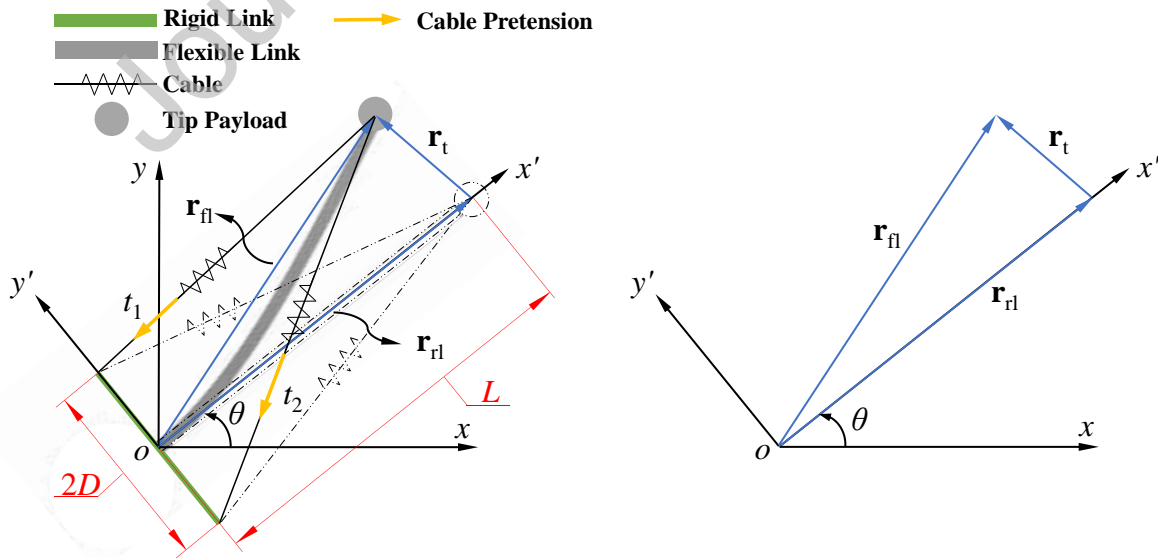
Fig. 1. Kinematic description of a single-link flexible mechanism with two pretensioned cables.

The actual location of a point on the flexible link is introduced by a rigid location from the undeformed link and a transversal deflection due to the bending flexibility. The rigid position vector of a point on the link is denoted as $\mathbf{r}_{rl}$. The transversal deflection vector with respect to the relative reference frame is defined as $^R\mathbf{r}_t = [0, v(s,t)]^T$, which is related to the rigid displacement of the point s and time t. Consequently, the location of the point on the link with respect to the global frame is given as follows

$$\mathbf{r}_{fl} = \begin{bmatrix} \cos\theta & -\sin\theta \\ \sin\theta & \cos\theta \end{bmatrix} \left(\begin{bmatrix} s \\ 0 \end{bmatrix} + \begin{bmatrix} 0 \\ v(s,t) \end{bmatrix} \right). \tag{1}$$

The potential energy of the system includes the potential energy of the flexible Euler-Bernoulli beam V_L, due to bending and the axial compression force exerted by an identical pre-tension T_{pre} in the two cables, and the potential energy of the cables. It is worth noting that the presence of a compression force F is produced by the two cable pretensions, which was not considered in the previous work [13] and exerts substantial influence on the beam potential energy. The axial strain of a flexible beam is expressed by the von Kármán nonlinearity through the nonlinear equation $\varepsilon_x = -yv' + (v')^2/2$ [47], where $v' = \partial v / \partial s$. Under the assumption that the transversal deformation v of the Euler-Bernoulli beam is small, the potential energy of the link from the cable pretension is given by taking into account the von Kármán nonlinearity as

$$V_L = \frac{EI}{2L^3} \int_0^1 \left(\frac{\partial^2 v}{\partial \zeta^2} \right)^2 d\zeta + \frac{1}{2L} \int_0^1 F \left(\frac{\partial v}{\partial \zeta} \right)^2 d\zeta, \tag{2}$$

where $s = \zeta L$, $\zeta \in [0,1]$, and F denotes the axial compression force on the flexible beam (i.e., $F < 0$) during the vibration of the beam. In accordance with the geometry of the layout shown in Fig. 1, the force F can be written as $F = 2T_{pre}L/\sqrt{D^2 + L^2}$. According to [23], the tension variation $\tau_{ac,i}$ of the i-th cable due to the traversal displacement v is given as

$$\tau_{ac,i} = kv(L,t)D/\sqrt{D^2 + L^2}, \qquad i = 1,2. \tag{3}$$

Moreover, each cable is modelled as a massless spring with an elastic coefficient k and a uniform cross-section. Under the assumption that both cables work at a given instant of time under the identical pretension $T_{pre} = k\Delta L(t)\big|_{t=0}$, the potential energy of the two cables is

$$V_C\big|_{t=0} = k \left(\Delta L(t)\big|_{t=0} \right)^2 = \frac{T_{pre}^2}{k}, \quad \Delta L(t)\big|_{t=0} = \sqrt{D^2 + L^2} - L_{free}, \tag{4.a}$$

$$V_C\big|_{t>0} = \frac{k}{2} \left(\Delta L(t)\big|_{t=0} - \Delta L(t)\big|_{t>0,s} \right)^2 + \frac{k}{2} \left(\Delta L(t)\big|_{t=0} + \Delta L(t)\big|_{t>0,e} \right)^2, \quad \text{if} \quad \Delta L(t)\big|_{t=0} > \Delta L(t)\big|_{t>0,s} > 0. \tag{4.b}$$

where $\Delta L(t)\big|_{t>0,e}$ denotes the approximate additional change of the extended cable length and is equal to $\sqrt{(\|v|_{s=L}\| + D)^2 + L^2} - \sqrt{D^2 + L^2}$ while $\Delta L(t)\big|_{t>0,s}$ is the retracted length of the other cable which is equal to $\sqrt{D^2 + L^2} - \sqrt{(D - \|v|_{s=L}\|)^2 + L^2}$. Additionally, L_{free} is the free length. It is assumed to be identical for the two cables. Since the transversal deformation $v|_{s=L}$ is small, the following expression is approximately obtained by neglecting the higher order terms of the transversal deformation expression.

$$\Delta L(t)\big|_{t>0,e} = \Delta L(t)\big|_{t>0,s} = \frac{D}{\sqrt{(D^2 + L^2)}} \|v(L,t)\|. \tag{5}$$

Substituting Eq. (4.a) and Eq. (5) into Eq. (4.b) yields

$$V_C\big|_{t>0} = \frac{T_{pre}^2}{k} + \frac{kD^2}{(D^2 + L^2)} v^2\big|_{s=L}, \quad \text{if} \quad \frac{T_{pre}}{k} > \frac{D}{\sqrt{(D^2 + L^2)}} \|v|_{s=L}\|, \tag{6}$$

where the inequality in Eq. (6) is a constraint between the lateral displacement and the pretension. When it is not valid, the cable tension will vanish because of the unidirectional nature of the cable force. Hence, the entire potential energy of the single-link flexible mechanism system with cables is expressed as

$$V(s,t) = V_L + V_C\big|_{t>0}. \tag{7}$$

In the following, the extended Hamilton's principle is applied to the single-link flexible mechanism as follows

$$\int_{t_1}^{t_2} (\delta T - \delta V + \delta W)dt = 0, \tag{8}$$

where δT and δW are the variation of the kinetic energy and the virtual work from the rotational motor torque (Appendix A). Subsequently, the variation of the potential energy in Eq. (7) is expressed as

$$\delta V = \delta V_{\mathrm{L}} + \delta V_{\mathrm{C}}|_{t>0}. \tag{9}$$

The two terms in the right hand side of Eq. (9) are written as

$$\delta V_{\mathrm{L}} = -\frac{EI}{L^3}\left[\left(\frac{\partial^2 v}{\partial \zeta^2}\right)\delta\left(\frac{\partial v}{\partial \zeta}\right)\Big|_{\zeta=0}^{\zeta=1} - \left(\frac{\partial^3 v}{\partial \zeta^3}\right)\delta v|_{\zeta=0}^{\zeta=1} + \int_0^1 \frac{\partial^4 v}{\partial \zeta^4}\delta v\, d\zeta\right] - \frac{F}{L}\left[\frac{\partial v}{\partial \zeta}\delta v|_{\zeta=0}^{\zeta=1} - \int_0^1 \frac{\partial^2 v}{\partial \zeta^2}\delta v d\zeta\right]d\zeta, \tag{10}$$

$$\delta V_{\mathrm{C}}|_{t>0} = -\frac{2kD^2}{D^2 + L^2}v|_{s=L}\delta v|_{s=L}. \tag{11}$$

After several mathematical manipulations (detailed in Appendix A), the dynamic model is developed by combining Eqs. (8) - (11)

$$\int_{t_1}^{t_2} A_1 \delta\theta \mathrm{d}t + \int_{t_1}^{t_2}\int_0^1 A_2 \delta v\, \mathrm{d}\zeta dt + \int_{t_1}^{t_2} A_3 \delta\left(\frac{\partial v}{\partial s}\right)\Big|_{s=L}\mathrm{d}t + \int_{t_1}^{t_2} A_4 \delta v|_{s=L}\mathrm{d}t$$
$$+ \int_{t_1}^{t_2}\left(-EI\left[\left(\frac{\partial^2 v}{\partial s^2}\right)\delta\left(\frac{\partial v}{\partial s}\right)\Big|_{s=0} - F\frac{\partial v}{\partial s}\delta v|_{s=0} + \left(\frac{\partial^3 v}{\partial s^3}\right)\delta v|_{s=0}\right]\right)\mathrm{d}t = 0. \tag{12}$$

The terms A_i in Eq. (12) are given by

$$A_1 = J_{\mathrm{m}}\left(\frac{\mathrm{d}^2\theta}{\mathrm{d}t^2}\right) + \tau + J_{\mathrm{p}}\left(\frac{\mathrm{d}^2\theta}{\mathrm{d}t^2} + \frac{\partial^3 v}{\partial s\partial t^2}\Big|_{s=L}\right) + m_{\mathrm{p}}(L^2 + v^2|_{s=L})\left(\frac{\mathrm{d}^2\theta}{\mathrm{d}t^2}\right) + \int_0^1 \rho\zeta L^2\left(\frac{\partial^2 v}{\partial t^2}\right)d\zeta + m_{\mathrm{p}}L\left(\frac{\partial^2 v}{\partial t^2}\right)\Big|_{s=L}$$
$$+ \int_0^1 \rho L v\left(\frac{\partial v}{\partial t}\right)d\zeta\left(\frac{\mathrm{d}\theta}{\mathrm{d}t}\right) + \int_0^1 \rho L[(\zeta L)^2 + v^2]\,d\zeta\left(\frac{\mathrm{d}^2\theta}{\mathrm{d}t^2}\right) + m_{\mathrm{p}}v|_{s=L}\left(\frac{\partial v}{\partial t}\right)\Big|_{s=L}\left(\frac{\mathrm{d}\theta}{\mathrm{d}t}\right),$$

$$A_2 = \frac{EI}{L^3}\frac{\partial^4 v}{\partial\zeta^4} + \rho L\left[\zeta L\left(\frac{\mathrm{d}^2\theta}{\mathrm{d}t^2}\right) + v\left(\frac{\mathrm{d}\theta}{\mathrm{d}t}\right)^2 + \left(\frac{\partial^2 v}{\partial t^2}\right)\right] - \frac{F}{L}\frac{\partial^2 v}{\partial\zeta^2},$$

$$A_3 = EI\left(\frac{\partial^2 v}{\partial s^2}\right)\Big|_{s=L} + J_{\mathrm{p}}\left(\frac{\mathrm{d}^2\theta}{\mathrm{d}t^2} + \frac{\partial^3 v}{\partial s\partial t^2}\Big|_{s=L}\right),$$

$$A_4 = m_{\mathrm{p}}L\left(\frac{\mathrm{d}^2\theta}{\mathrm{d}t^2}\right) + m_{\mathrm{p}}\left(\frac{\partial^2 v}{\partial t^2}\right)\Big|_{s=L} - EI\left(\frac{\partial^3 v}{\partial s^3}\right)\Big|_{s=L} + F\frac{\partial v}{\partial s}\Big|_{s=L} + \frac{2kD^2}{D^2 + L^2}v|_{s=L}. \tag{13}$$

The last term in Eq. (12) is always equal to zero as a result of the boundary conditions mentioned below at $s = 0$. Since the four variations $\delta\theta, \delta v, \delta\left(\frac{\partial v}{\partial s}\right)\Big|_{s=L}$ and $\delta v|_{s=L}$ are independent, the expressions of A_1, A_2, A_3, and A_4 in Eq. (13) are all equal to zero. Hence, the dynamical model of a single-link flexible mechanism with two pretensioned cables is given by

$$J_{\mathrm{m}}\left(\frac{\mathrm{d}^2\theta}{\mathrm{d}t^2}\right) + \tau + J_{\mathrm{p}}\left(\frac{\mathrm{d}^2\theta}{\mathrm{d}t^2} + \frac{\partial^3 v}{\partial s\partial t^2}\Big|_{s=L}\right) + m_{\mathrm{p}}(L^2 + v^2|_{s=L})\left(\frac{\mathrm{d}^2\theta}{\mathrm{d}t^2}\right) + \int_0^1 \rho\zeta L^2\left(\frac{\partial^2 v}{\partial t^2}\right)d\zeta + m_{\mathrm{p}}L\left(\frac{\partial^2 v}{\partial t^2}\right)\Big|_{s=L}$$
$$+ \int_0^1 \rho L v\left(\frac{\partial v}{\partial t}\right)d\zeta\left(\frac{\mathrm{d}\theta}{\mathrm{d}t}\right) + \int_0^1 \rho L[(\zeta L)^2 + v^2]\,d\zeta\left(\frac{\mathrm{d}^2\theta}{\mathrm{d}t^2}\right) + m_{\mathrm{p}}v|_{s=L}\left(\frac{\partial v}{\partial t}\right)\Big|_{s=L}\left(\frac{\mathrm{d}\theta}{\mathrm{d}t}\right) = 0, \tag{14}$$

$$EI\frac{\partial^4 v}{\partial s^4} + \rho\left[s\left(\frac{\mathrm{d}^2\theta}{\mathrm{d}t^2}\right) + v\left(\frac{\mathrm{d}\theta}{\mathrm{d}t}\right)^2 + \left(\frac{\partial^2 v}{\partial t^2}\right)\right] - F\frac{\partial^2 v}{\partial s^2} = 0, \tag{15}$$

$$EI\left.\left(\frac{\partial^2 v}{\partial s^2}\right)\right|_{s=L} + J_{\mathrm{p}}\left(\frac{\mathrm{d}^2\theta}{\mathrm{d}t^2} + \left.\frac{\partial^3 v}{\partial s \partial t^2}\right|_{s=L}\right) = 0, \tag{16}$$

$$m_{\mathrm{p}}L\left(\frac{\mathrm{d}^2\theta}{\mathrm{d}t^2}\right) + m_{\mathrm{p}}\left.\left(\frac{\partial^2 v}{\partial t^2}\right)\right|_{s=L} - EI\left.\left(\frac{\partial^3 v}{\partial s^3}\right)\right|_{s=L} + F\left.\frac{\partial v}{\partial s}\right|_{s=L} + \frac{2kD^2}{D^2+L^2}v|_{s=L} = 0. \tag{17}$$

Since the proximal end of the flexible link is fixed to the rotational axis, the beam is clamped at $s = 0$ and the resulting boundary conditions are expressed as follows

$$v|_{s=0} = 0, \qquad \left.\frac{\partial v}{\partial s}\right|_{s=0} = 0. \tag{18}$$

Moreover, another boundary condition at $s = L$ is obtained in Eqs. (16) and (17), which represent the moment and force constraints of the cable-stiffened flexible beam respectively.

3. Critical cable pretension for buckling phenomenon

For the small amplitude free oscillation of the cable-stiffened beam, the lateral deformation $v(s, t)$ is assumed to be separable in space and time as follow,

$$v(s, t) = \Psi(s)\sin(\omega t) \tag{19}$$

where $\Psi(s)$ is a function of the location s of the curvilinear points and ω is a pulsation that has to be determined. By substituting of Eq. (19) into Eq. (15), the following equation is obtained

$$EI\frac{\mathrm{d}^4\Psi}{\mathrm{d}s^4}\sin(\omega t) - \rho\Psi(s)\omega^2\sin(\omega t) - F\frac{\mathrm{d}^2\Psi}{\mathrm{d}s^2}\sin(\omega t) = 0, \tag{20}$$

where $\frac{\mathrm{d}\theta}{\mathrm{d}t}$ and $\frac{\mathrm{d}^2\theta}{\mathrm{d}t^2}$ are set to zero since the free oscillation begins when the motor stops rotating. Compared to [13], the last term is added due to the applied axial beam compression force induced by the cable pretensions. Considering the generalized case, Eq. (20) leads to

$$EI\frac{\mathrm{d}^4\Psi(s)}{\mathrm{d}s^4} - \omega^2\rho\Psi(s) - F\frac{\mathrm{d}^2\Psi(s)}{\mathrm{d}s^2} = 0. \tag{21}$$

The buckling of the flexible beam occurs when the cable tensions attain the critical values, which causes the beam instability with a time-independent equilibrium of Eq. (21) as detailed in [48]. Moreover, the first natural frequency of the cable-stiffened beam is equal to zero when the critical cable pretension is applied [49]. In order to avoid structural instability, it is thus of significant importance to determine the critical cable pretension before discussing the effect of pretension on the dynamic characteristics of a cable-stiffened flexible beam.

Referring to [48], when the structural buckling occurs, the first natural frequency of the system is equal to zero. Accordingly, the time-independent equilibrium of the system is written as

$$EI\frac{\mathrm{d}^4\Psi(s)}{\mathrm{d}s^4} - F\frac{\mathrm{d}^2\Psi(s)}{\mathrm{d}s^2} = 0. \tag{22}$$

Subsequently, recalling that the axial compression load satisfies $F < 0$, the characteristic eigenvalue equation of Eq. (22) is deduced as

$$EIr^4 - Fr^2 = 0, \tag{23}$$

and the solutions are $r_1 = r_2 = 0$, $r_3 = i\sqrt{\frac{-F}{EI}}$, $r_4 = -i\sqrt{\frac{-F}{EI}}$, where i denotes the imaginary unit. Thus, the general solution of Eq. (23) is obtained as

$$\Psi(s) = C_1 + C_2 s + C_3\sin(\beta s) + C_4\cos(\beta s), \tag{24}$$

where $\beta = \sqrt{\frac{-F}{EI}}$. Substituting Eq. (24) into the boundary constraints Eqs. (16) and (18), the following equation system is obtained

$$\begin{bmatrix} 0 & 0 & F\sin(\beta L) & F\cos(\beta L) \\ 1 & 0 & 0 & 1 \\ 0 & 1 & \beta & 0 \end{bmatrix} \begin{bmatrix} C_1 \\ C_2 \\ C_3 \\ C_4 \end{bmatrix} = \mathbf{0}_{3\times 1}. \tag{25}$$

After mathematical manipulations, the unknown vector is obtained as $[C_1 \quad C_2 \quad C_3 \quad C_4]^{\mathrm{T}} = C_3[\tan(\beta L) \quad -\beta \quad 1 \quad -\tan(\beta L)]^{\mathrm{T}}$. Moreover, it can be deduced from Eqs. (17) and (24) that

$$FC_2 + \frac{2D^2 k}{D^2 + L^2}(C_1 + C_2 L) = 0. \tag{26}$$

which, by means of the above vector, can be written as

$$\left\{ -\beta F + \frac{2D^2 k}{D^2 + L^2}[\tan(\beta L) - \beta L] \right\} C_3 = 0. \tag{27}$$

From the non-trivial solution of Eq. (27), the eigenvalue equation is obtained when the unknown C_3 is supposed to be nonzero. In fact, the following transcendental equation on the critical axial compression load is obtained by setting the first expression in Eq. (27) to zero

$$\cot(\beta L) = \frac{2\lambda k}{(2\lambda k L + F)\beta}, \tag{28}$$

where $\lambda = D^2/(D^2 + L^2)$. It is worth noting that the critical force for the flexible beam with cables is related to both the geometric parameters (e.g., D and L) and the material properties of both the flexible beam and the cables (e.g., EI and k). Obviously, the coupling effect of the cable-beam interaction is also exhibited in Eq. (28). Moreover, it should be noted that the mass of the tip mass is not included in Eq. (28), which indicates that the tip mass does not affect the value of the buckling force in the framework of this study and is validated in the simulation experiments in Sect.5. In comparison to the classical formula of the critical axial compression force from Euler formulation, namely $F = \pi^2 EI/(\mu L)^2$ with the factor $\mu = 2$ in the fixed-free end connection scenario, it leads to $\cos(\beta L) = 0$ in agreement with Eq. (28) when D is set to zero (i.e., $\lambda = 0$).

The critical force for the single flexible beam with cables is determined by the first intersection point of the expressions on both sides of Eq. (28). For example, the geometric and physical parameters of a specific flexible beam with cables are summarized in Tab. 1. As shown in Fig. 2, the critical buckling force can be determined with an arror. Consequently, the fsolve function in Matlab is utilized to solve the nonlinear equation of Eq. (28) and the critical force is identified as -9.87 N. As a result, the pretension of the cables can be calculated by $F = 2T_{\mathrm{pre}}L/\sqrt{D^2 + L^2}$ as $T_{\mathrm{pre}} = 5$ N based on the initial system configuration.

Table 1. Geometric and physical parameters of a flexible-link mechanism with Nylon cables and the flexible link made of steel.

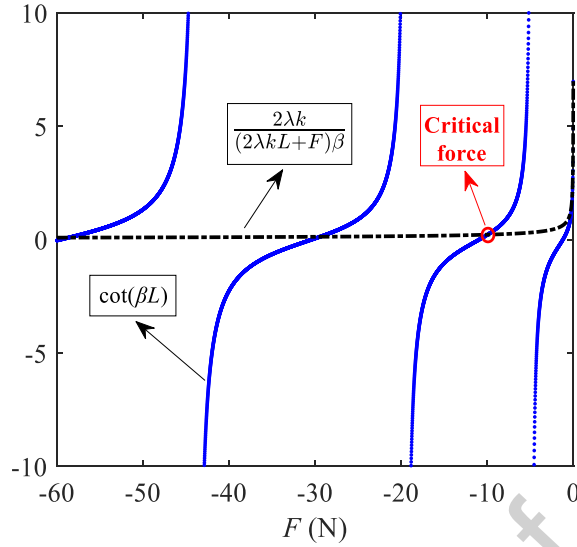| Item	Parameter	Value
Link bending stiffness ($\mathrm{N \cdot m^2}$)	EI	0.1775
Link length (m)	L	0.6
Rigid link length (m)	D	0.1
Spring coefficient of cables (N/m)	k	3700

Fig. 2. Critical force determination of a single-link flexible mechanism with two cables.

For the purpose of investigation of the effect of geometric and material parameters on the critical cable pretension, a non-dimensional parameter is defined as $D^* = D/L$. As a result, different values of D^* reveal the effects of various cable layouts/inclinations. Following [50-52], the cable spring coefficient is $k = E_c A_c/L_c$, where E_c is the elastic modulus and A_c the cross-sectional area along with the cable stretched length $L_c = L\sqrt{D^{*2}+1}$. The relationship between the critical force F and D^* is depicted in Fig. 3, where the considered cable materials are Nylon, Steel and Polyethylene whose elastic modulus are given in Tab. 2. It is clearly observed that the critical force F is equal to 1.22 N with $D^* = 0$ for all three types of cables. As mentioned before, the magnitude of the critical force $F|_{D^*=0}$ merely depends on the length and the bending stiffness of the flexible beam. Moreover, the critical force soars as D^* increases and then decreases as shown in Fig. 3. Recalling Eq. (28), the latter is simplified as $\cot(\beta L) = \frac{2\lambda|_{D^*\to\inf}k|_{D^*=\inf}}{(2\lambda|_{D^*\to\inf}k|_{D^*\to\inf}L+F)\beta} = 0$ with $\lambda|_{D^*\to\inf} = 1$ and $k|_{D^*\to\inf} = 0$. As a consequence, it is readily observed that the critical force under the extreme condition $D^* \to \inf$ is equal to $F|_{D^*\to\inf} = \pi^2 EI/(2L)^2$. However, it is difficult to derive the analytical solution formulation of D^* to the maximum critical force because of the transcendental relationship between βL and λk in Eq. (28). Overall, it can be noted that a large cable elastic modulus corresponds to a large critical force for the same value of D^* but the maximum critical force is obtained with a relatively small D^* for the three presented cable materials. It is also worth noting that the cables cannot be modelled as massless springs when D^* becomes very large. Indeed, sagging effect due to the cable own mass and torsional stiffness should be carefully tackled in the case of long cables [53,54].
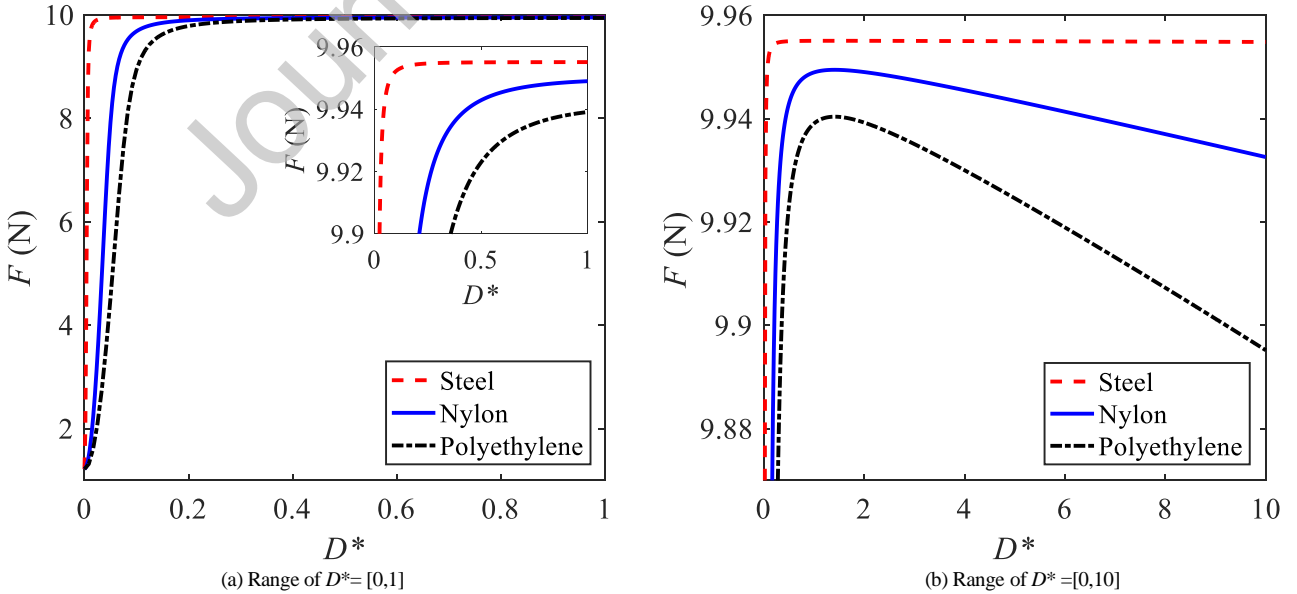

(a) Range of D^*= [0,1]

(b) Range of D^* =[0,10]

Fig. 3. Change of the critical force F with respect to D^* using cables made of nylon, steel and polyethylene (the beam length is $L = 0.6$ m).

Table 2 Elastic modulus of nylon, steel and polyethylene for cables (Unit: GPa).

Material	Nylon	Steel	Polyethylene
Elastic Modulus	2.83	207	1.1

Moreover, another non-dimensional parameter is defined as $\chi = \frac{EI}{E_c A_c L^2}$. It is the ratio of the beam flexural stiffness over the cable axial stiffness. The resultant critical forces with respect to χ varying within a technical relevant range of $[0.5, 2.5] \times 10^{-4}$ are presented in Fig. 4. Similar to D^*, the beam material plays a significant role in the buckling phenomenon of this flexible beam with cables. It can be observed that the force monotonically increases as χ becomes larger for various D^*. Indeed, a large χ corresponds to a beam made of a material with high elastic modulus and a larger buckling load is thus required to make the system unstable.
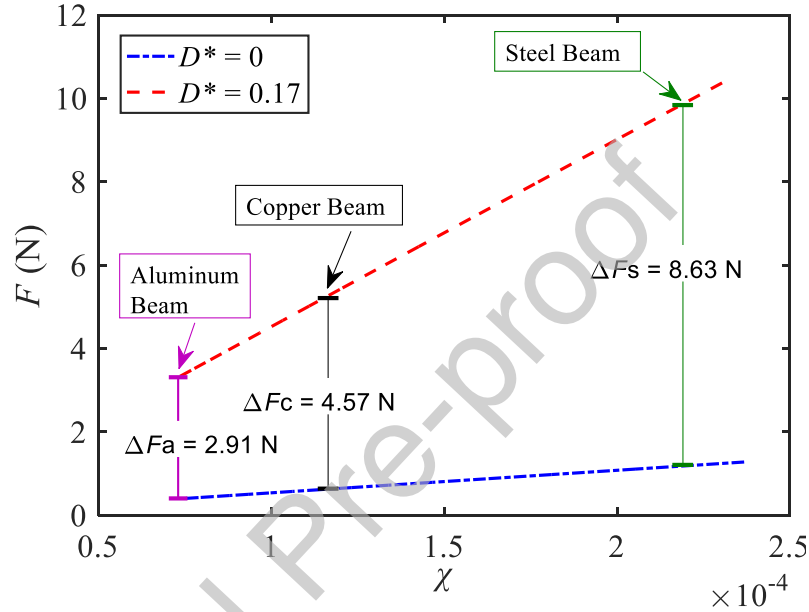
Fig. 4. Change of the critical force F with respect to χ (beam length $L = 0.6$ m and cables made of Nylon).

For example, three types of common metallic materials for the beam as listed in Tab. 3 are discussed with the cables made of Nylon. The three vertical lines shown in Fig. 4 stand for the three materials of the beams, namely a steel beam in green, a copper beam in black and an aluminum beam in violet. The intersection points of the vertical lines and each curve are referred to as the critical forces with corresponding material and D^* given in Table 4. The obtained magnitudes of the critical forces with $D^* = 0$ are consistent with those from the classical beam equation $F = \pi^2 EI / (2L)^2$. More importantly, the results reveal that the influence of D^* decreases for a more compliant beam since the relative values of critical forces for two D^* shrink as χ reduces. In other words, the critical force of the cable-stiffened beam asymptotically approaches that of the cantilever beam for vanishing χ (i.e., the beam flexural stiffness is much lower than the axial cable stiffness).

Table 3 Elastic modulus of copper, steel and aluminum for the beam (Unit: GPa).

Material	Steel	Copper	Aluminum
Elastic Modulus	207	110	69

Table 4 Critical force for beams made of steel, copper and aluminum (Unit: N).

D^*	Critical force		
	Steel	Copper	Aluminum
0	1.21	0.64	0.40
0.17	9.84	5.21	3.31

As depicted in Fig. 4, the effect of the parameter D^* on the critical force of the flexible system is important as well. Taking the flexible beam made of steel as an example, a group of different values of parameter D^* are selected and the corresponding critical forces together with the cable tensions are shown in Fig. 5. Both the critical force and the cable tension increase quickly in the beginning. The effect of D^*

on the critical buckling load is negligible when D^* becomes larger than 0.2. However, the cable tension related to the critical force will increase gradually since the angle between the cable and the beam has a considerable influence on the determination of the cable tension.
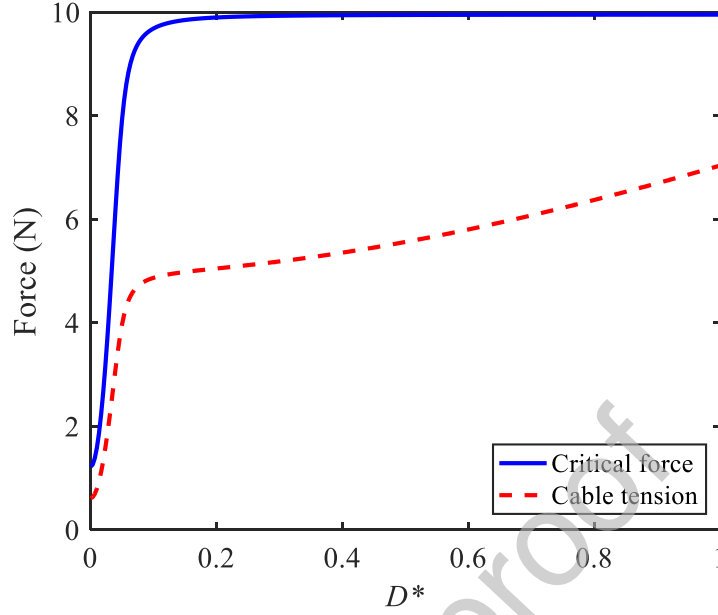

Fig. 5. Critical force and cable tension with respect to D^* (beam length $L = 0.6$ m and cables made of Nylon).

4. Lateral stiffness

The lateral instability of a flexible column or beam depends on its axial loading. The critical buckling force is defined as the exact value of the axial loading that makes the column laterally unstable. Referring to [32,55,56], the lateral stability capacity of an unbraced column and beams can be assessed using lateral stiffness with the definition of lateral resistance subjected to variable lateral forces. Moreover, the critical buckling load can be identified when the lateral stiffness of the column is equal to zero. The post-buckling of a clamped rod is investigated with the Ramberg-Osgood constitutive law in [57], which is applied to design column structures under large deformation. Different from the unbraced columns, this paper focuses on a more complex structure by considering the influence of the cables on a flexible beam. Hence, the lateral stiffness for the flexible single column with two cables is deduced in this section.

The beam-column connection rigidity plays a significant role in estimating the critical buckling loads of columns. The concept of the end-fixity factor is introduced to define the relative stiffness at a connection end [55,56]. For a clamped end, the value of the end-fixity factor is equal to zero while it is unity for a free end or an ideally pinned connection end. Regarding the system in the current study, the lateral stiffness expression of a flexible single beam with the axial loads from the cable pretension is given as

$$k_1 = \frac{-F\beta\cos(\beta L)}{-(\beta L)\cos(\beta L) + \sin(\beta L)}, \tag{29}$$

where k_1 denotes the lateral stiffness of the flexible beam and the axial compression load F together with the variable β defined in Eq. (24). For the sake of brevity, the detailed derivation of this equation is omitted here. Next, the contribution of the cables to the lateral stiffness of the system is taken into account and integrated with an improved formulation.

As illustrated in Fig. 6, a lateral deflection v is caused by the different cable tensions at the tip end of the flexible beam. In fact, the lateral deformation is very small and can be considered as elastic bending (it is exaggerated for illustration purposes in Fig. 6). At the initial instant, two cable pretensions are equal to an identical force T_{pre}. After adding the cable tensions, a lateral deflection occurs such that the tensions begin to vary correspondingly. Under the assumption of the massless spring with a constant elastic coefficient, the tension variations of the upper and lower cables can be obtained as

$$\delta T_{c1} = T_1 - T_{pre}, \delta T_{c2} = T_2 - T_{pre}. \tag{30}$$

According to Eq. (3), the two cable tension variations are given as

$$\delta T_{c1} = -k\sqrt{\lambda}|v|, \delta T_{c2} = k\sqrt{\lambda}|v|, \tag{31}$$

where $\lambda = D^2/(D^2 + L^2)$ and v denotes a small lateral displacement shown in Fig. 6. Consequently, the lateral components of the cable tensions along the y-axis direction (i.e., lateral direction) can be deduced using trigonometric relationship as

- 12 -

$$\delta T_{\text{lc1}} = -k\lambda|v|, \delta T_{\text{lc2}} = k\lambda|v|. \tag{32}$$

Based on Eqs. (30) to (32), the corresponding components of lateral stiffnesses provided by the two cables are

$$k_{\text{lc1}} = \frac{\delta T_{\text{lc1}}}{-|v|} = k\lambda, k_{\text{lc2}} = \frac{\delta T_{\text{lc2}}}{|v|} = k\lambda. \tag{33}$$

Therefore, the complete lateral stiffness expression for the flexible single link with two cables can be rewritten as

$$k_{\text{ls}} = k_{\text{l}} + k_{\text{lc1}} + k_{\text{lc2}} = \frac{-F\beta\cos(\beta L)}{-(\beta L)\cos(\beta L) + \sin(\beta L)} + 2k\lambda, \tag{34}$$
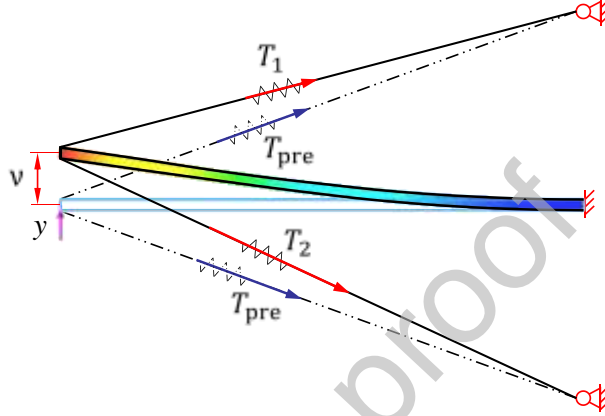

Fig. 6. Illustration of lateral deflection under different cable tensions.

In accordance with the Storey-buckling method for determining the critical buckling load, once the lateral stiffness of the beam with cables reduces to zero, the buckling phenomenon is about to occur. After several mathematical manipulations (Appendix B), the formulation to predict the critical buckling load is the same as Eq. (28), which further demonstrates the effectiveness of the method proposed in Section 4. More importantly, the dynamic modelling using the extended Hamilton's principle can be applied to further investigate a dynamic characterization through modal analysis for the single-link flexible system with two cables besides the determination of buckling loads.

5. Simulation

In this section, a series of simulations are implemented in ANSYS with the aim of validating the method proposed in the previous sections. A finite element model of the single-link flexible system with two cables is created in ANSYS as illustrated in Fig. 7. In accordance with the previous assumption, the cables are represented by two massless springs with an identical elastic coefficient k. It is worth noting that, in ANSYS, the springs are set to tension only to mimic the unilateral nature of cable forces. A tip mass is attached to the free end of the flexible beam. However, the rigid link of Fig. 1 is neglected and replaced by a frame to mount both the beam and the cables. Considering that the mechanism moves in the horizontal plane and the fact that it has negligible deflection against gravity due to the high stiffness along the vertical plane, the effect of gravity is neglected as well.
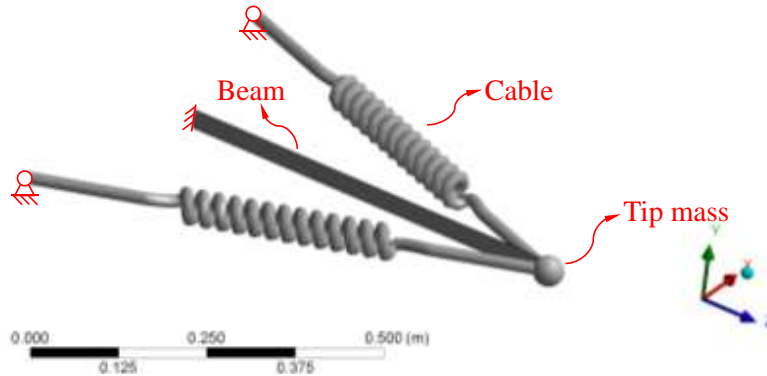

Fig. 7. Layout of the simulation model in ANSYS software.

- 13 -

As expected, the tip mass does not exert any influence on the determination of the critical buckling force in the simulation, which is consistent with the conclusions on the basis of Eq. (28). More importantly, the critical bucking force of the flexible link system with cables is obtained based on the eigenvalue buckling module of ANSYS. The resulting D^* obtained from the simulations are compared with those obtained using Eq. (28) of the proposed method. The relative error of the critical buckling forces is defined as $(F_{simulation} - F_{calculation})/F_{simulation}$. As shown in Fig. 8, it can be clearly observed that the forces match very well in the given range of values of the non-dimensional parameter D^* defined in Section 2, whereas the relative errors grow and stay around 2% with D^* larger than 0.1. The simplicity of von Kármán nonlinearity in Eq. (2) without considering the width of the beam may account for the discrepancy between the results from the proposed method and the simulations. Furthermore, the reduction of the critical force as D^* reaches a higher value has been validated, which is in good agreement with the calculated results depicted in Fig. 8(b). In addition, the value of the tip mass is changed to testify its effect on the evaluation of critical buckling loads. It turns out that the buckling load is not affected by the tip payload, which is consistent with the analytical results. Therefore, the simulation results demonstrate the validity of the proposed method for predicting the critical buckling force in this system, which also gives a more conservative cable pretension values compared to the simulation results in order to avoid the occurrence of buckling phenomenon of a flexible beam with cables.

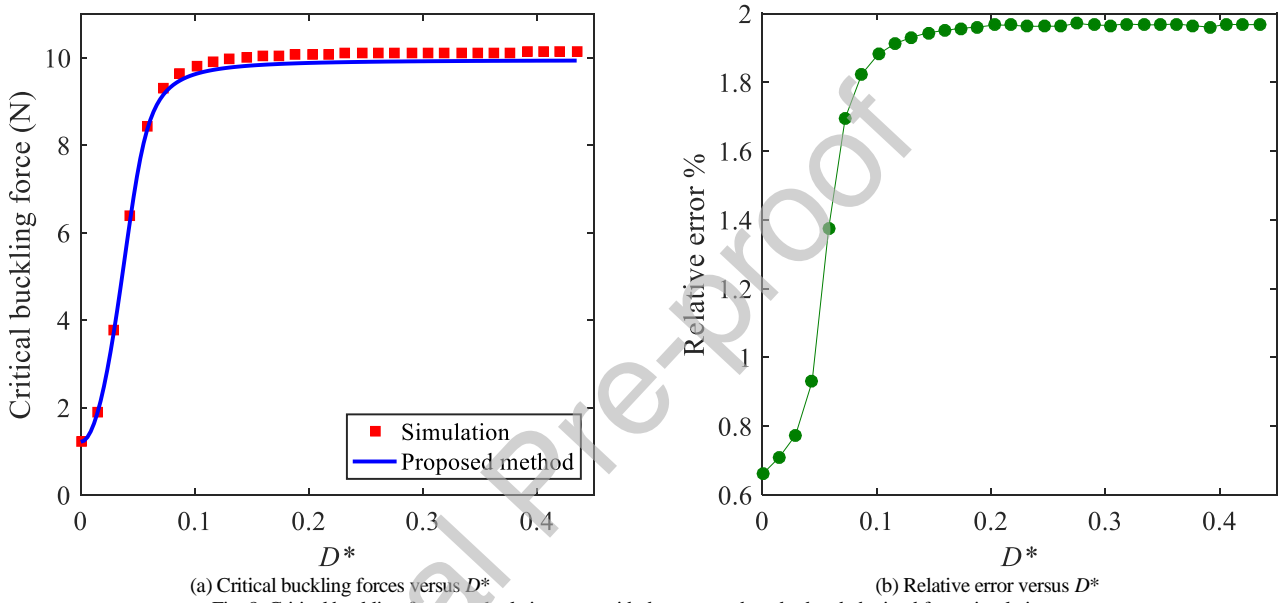(a) Critical buckling forces versus D^* (b) Relative error versus D^*

Fig. 8. Critical buckling forces and relative error with the proposed method and obtained from simulation.

In addition, a procedure, similar to the buckling force identification method presented in [32], is accomplished with the simulation model in ANSYS. The basic principle is to determine the critical forces using a linear extrapolation when the lateral stiffness of the tip end of the beam reaches zero. The main procedure can be summarized as follows:

(1) Select several different sets (5 sets here) of cable pretensions, which are lower but close to the theoretical maximum cable tension corresponding to buckling;

(2) Impose a constant force in the x-axis direction of the global frame (shown in Fig. 7) at the tip end of the beam. This force is selected according to the pretension value;

(3) Measure the correspondent lateral displacement and calculate the lateral stiffness of the system at the tip end;

(4) Predict the critical buckling force using a linear extrapolation as the lateral stiffness is equal to zero.

Before implementing the simulation testing, it should be acknowledged that the aforementioned procedure obtains an approximate force due to the simplicity of the linear fitting between the lateral stiffness and the axial loading at the beam. However, the accuracy of the procedure can be improved by the adjustment of the lateral forces for different loadings. As for the configuration with the pulley located at D = 0.1 m, the specification of the procedure and the results are summarized in Table. 5. Based on the least-squares fitting theory, a linear fitting line as shown in Fig. 9 is determined as $F_{al}=10.39 - 0.006542 \times k_1$ with the root mean square error equal to 0.02882. Finally, the critical buckling force for the present configuration is estimated to be 10.39 N. The relative error between the identified force and the calculated force is obtained as 5.6%. Additionally, the relative error between the identified force and the obtained force from the eigenvalue buckling module of ANSYS is 2.8%, which suggests that the above-mentioned procedure is a feasible method to predict the approximate critical buckling load. However, it also needs to be noticed that this approach highly depends on the measurement accuracy of both the lateral external force and the lateral deflection, which hinder the experimental demonstration in practice due to the cable compliance and hybrid compliance associated with the flexible beam. More importantly, the detailed expression of the obtained linear fitting line varies in accordance with the predefined lateral external forces and the cable pretensions. As a result, this procedure has been applied as a supplementary method to validate the critical buckling force of the flexible link with two cables only in the simulation environment.

- 14 -

Table 5 Feasible pairs of tensions for the determination of the critical force.

Simulation No.	1	2	3	4	5
Pretension (N)	4.92	4.94	4.96	4.98	5.0
Axial load (N)	9.702	9.742	9.781	9.821	9.860
Lateral external force (N)	0.005	0.004	0.002	0.0015	0.001
Lateral deflection (m)	4.96×10^{-5}	4.06×10^{-5}	2.1×10^{-5}	1.63×10^{-5}	1.27×10^{-5}
Lateral stiffness (N/m)	100.7	98.6	95.2	92.2	78.5
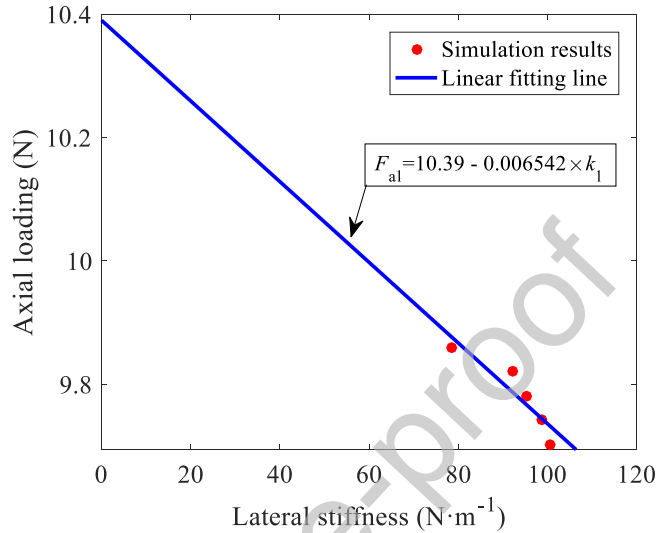
Fig. 9. Linear extrapolation for identification of the critical buckling force.

$$F_{al}=10.39 - 0.006542\times k_l$$

6. Experimental verification

The experimental testbed is shown in Fig. 10. One end of each cable is attached at the tip end of a flexible link made of steel, whereas the other cable end is connected to a force sensor (HBM U9C) through a pulley. There is a mobile frame supported by a wheel jack to adjust the cable tensions. The beam and the two pulleys are mounted on the mobile frame, while the force sensors are located at the base. In the experimental setup, the variations of the tensions in the two cables are measured by means of the force sensors and recorded with the use of a data acquisition equipment (Beckhoff CX5100). The height of the mobile frame can be adjusted with the actuation of the wheel jack and therefore the cable tensions will change accordingly due to the constant length of the cables.

To verify the effect of the location of the pulleys on the critical buckling force of the flexible link system, a set of five distinct points denoted as {1#,2#,3#,4#,5#} are selected with specific distances depicted in Fig. 11. It can be noted that the pair of pulleys are always fixed symmetrically to the vertical middle plane of the beam. The tip mass is split in two identical masses attached on both sides of the free end of the beam.
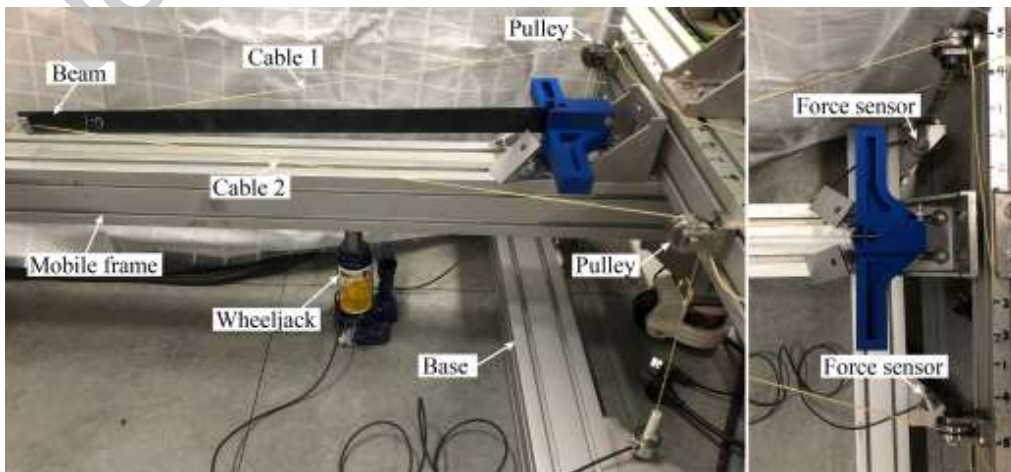

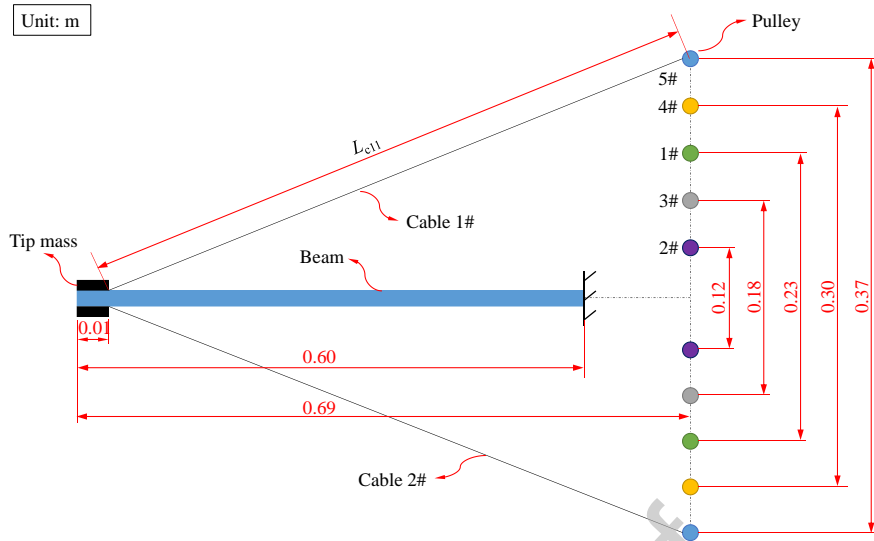Fig. 10. Testbed for verification of the effects of the cable pretensions.

Fig. 11. Layout of five pulley locations for the flexible beam with two cables (dimensions in meters).

Under the assumption that the tip mass is a rigid body with length of 0.01 m, the value of the actual beam length in the experiment is taken as $L = 0.59$ m. Subsequently, the cable spring coefficient can be calculated by $k = EA/L_C$ where L_C denotes the length of the cable from the cable attachment at the tip mass to the anchor point at the force sensor. The value of the free length of the i-th cable is set to $L_{Ci} = L_{Ci1} + L_{Ci2}$ in which L_{Ci1} is the cable length in the horizontal plane shown in Fig. 11 and L_{Ci2} is the cable length between the pulley and the force sensor. In this paper, L_{Ci2} is equal to 0.21 m in the experiments and the cable free length L_{Ci} is equal to $L_{Ci1} + 0.21$. For example, in the case of pulleys at position 1#, the free lengths of both cables are $L_C = 0.9$ m. As a result, the corresponding spring coefficient is obtained as $k = 2470$ N/m. According to Eq.(28) in Sect. 3, the theoretical buckling load of the system at position 1# is 9.82 N and therefore the maximum pretension is constrained to be lower than 5 N. Based on the simulation model in Fig. 7, the critical buckling load is estimated as being equal to 9.98 N, which is slightly larger than the value obtained with the proposed analytical method.
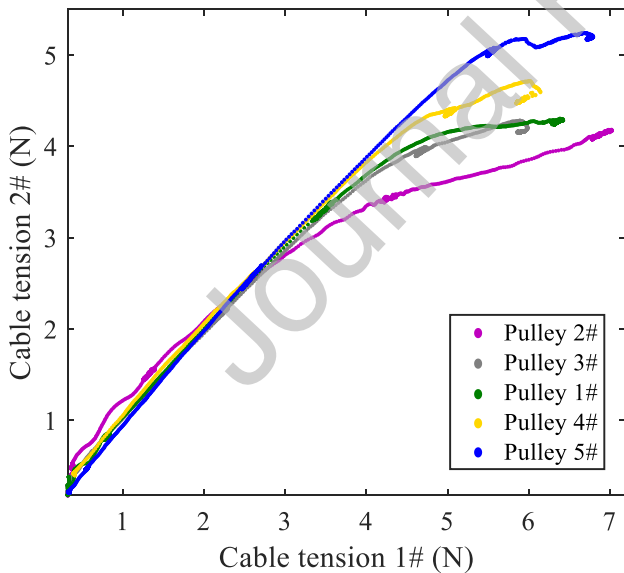

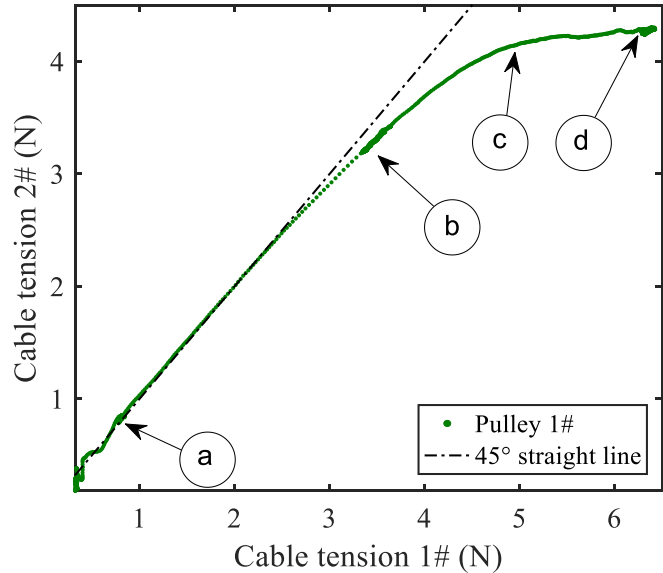Fig. 12. Changes in the cable tensions associated with five pulley locations during loading.

Fig. 13. Changes in the cable tensions associated with the pulley location 1#.

As depicted in Fig. 12, the variations of the cable tensions are recorded for five locations of the pulleys. A similar trend is followed in all five scenarios. At first, the two cable tensions increase with almost the same value under the actuation of the wheel jack. During this stage, it can be clearly observed that a small oscillation of the cable tensions happens due to the compliance of the beam. In particular, these vibrations take place more obviously when the location of the pulley is closer to the middle plane of the beam, namely for a small D. It can be explained by the fact that a large angle between the beam and the cables makes the system stiffer. As the cable tensions increase, the difference between the two cable tensions increases correspondingly, which means that the beam bending becomes more significant. When

cable tensions become very high, a nonlinear relationship between the two cable tensions can be seen. Taking the pulley location 1# as an example, four typical instants {a, b, c, d} during the loading are presented in Fig. 13. The corresponding snapshots of the non-buckling or buckling beam together with the specified tensions are shown in Fig. 14.
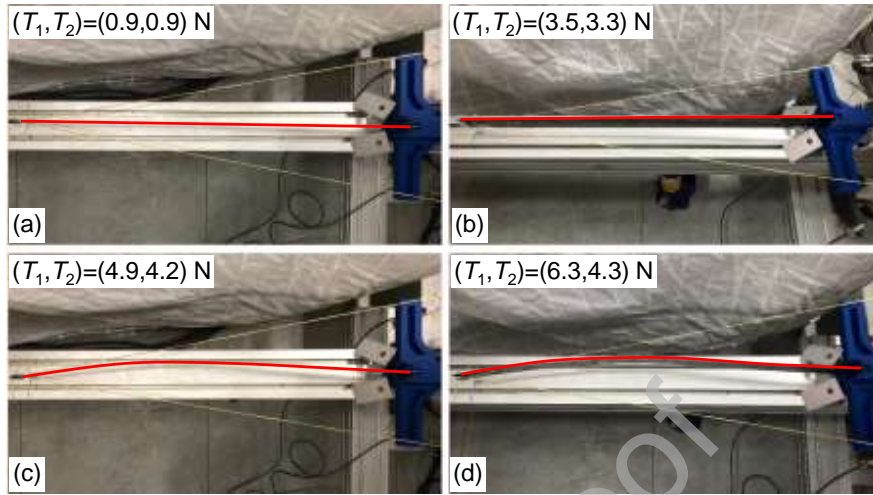

Fig. 14. Buckling phenomenon of the flexible beam with cables during loading.

From Fig. 13 and Fig. 14, the following observations can be made on the buckling of the flexible single beam with two cables. Tension oscillation exists before the instant (a), which is mainly due to both the assembly errors and instability of the initial cable elongation. During the period from instant (a) to the instant before (b), the two cable tensions change with almost identical values and the flexible beam remains straight like at the instant (a). Then, the tension curve starts to deviate from the 45° straight line and the tension difference rises as the loading continues (e.g., 0.2 N at the instant (b) and 0.7 N at the instant (c)). However, the flexible beam still remains straight at instant (b), while it begins to buckle from instant (c) on. It is worth noting that the beam deflection is larger at the points near the middle section of the beam at instants (c) and (d). In comparison, the maximum lateral deflection of the middle point at instant (c) is smaller than that at instant (d). It indicates that a higher tension deviation results in a large lateral deflection of the beam. Although the lateral deviations can be readily measured by means of a laser displacement sensor, it remains difficult to determine the exact value of the critical buckling force associated with the pulley location 1#. Nevertheless, it has been discovered that using a small lateral force, the flexible beam can change easily to the mirror shape with reference to its initial middle plane at the instant (c). Moreover, the beam deformation at the instant (d) is larger than that at instant (c), where the axial force (*i.e.*, 10.45 N) from the two cable tensions is higher than the critical buckling force determined by the simulation and the proposed method.

To summarize, the three buckling loads obtained respectively from the analytical method, the simulation and the experiments are compared in Tab. 6. It should be noted that the maximum cable pretension from the experiment results is approximated as the average of two cables tensions at the instant (c). Accordingly, the buckling load of the cable-beam system in the pulley configuration 1# is calculated as 8.94 N. The relative errors with respect to the experimental value of buckling loads are 9.8% for the analytical value and 11.6% for the simulation. The discrepancy may result from the inaccuracy of the experimental assembly where the flexible beam is connected to two cables.

Table 6 Comparison of buckling loads and the maximum cable pretension at position 1# (Unit: N).

Method	Buckling load	Max. cable pretension
Analytical	9.82	5
Simulation	9.98	5.08
Experiment	8.94	4.55

7. Conclusions

In this paper, the Hamilton's extended principle is adopted to develop the dynamical model of a single-link flexible system with two pretensioned cables. A transcendental equation involving bending stiffness and length of the beam as well as spring coefficient and locations of the cables is obtained for the determination of the buckling load. Analytical results show that the buckling load for several specific cable configurations is consistent with that from classic formula of a flexible beam with the fixed-free end connections. The transcendental equation is also derived from the concept of lateral stiffness. Buckling phenomenon occurs once the value of lateral stiffness reduces to zero. The complete lateral stiffness is composed by the flexible link stiffness and the one induced by the pretensioned cables. The variation

- 17 -

of the buckling load with respect to the location of the two cable pulleys based on the dynamical model is demonstrated by the ANSYS simulations. Finally, experiments are conducted on a physical testbed. Buckling of the flexible beam is documented and presented with several snapshots. Further research will focus on the effect of cable pretensions on the dynamic characteristics of the single-link flexible system with two cables within the critical buckling loads.

Declaration of Competing Interest

The authors declare that they have no competing interests.

Acknowledgment

Appendix A

According to Eq. (1), the position vector of a point s on the link with respect to the inertial frame is given by

$$\mathbf{r}_{\mathrm{fl}} = \begin{bmatrix} s\cos\theta - v(s,t)\sin\theta \\ s\sin\theta + v(s,t)\cos\theta \end{bmatrix}. \tag{A.1}$$

Then, the kinetic energy of the single flexible link is obtained as

$$T_{\mathrm{L}} = \frac{\rho L}{2}\int_0^1 \left(\frac{\partial \boldsymbol{r}_{\mathrm{fl}}}{\partial t}\right)^{\mathrm{T}}\left(\frac{\partial \boldsymbol{r}_{\mathrm{fl}}}{\partial t}\right)\mathrm{d}\zeta\,, \tag{A.2}$$

and the partial derivative of the position vector $\mathbf{r}_{\mathrm{fl}}$ with respect to time t is calculated from Eq. (A.1) as follows

$$\frac{\partial \boldsymbol{r}_{\mathrm{fl}}}{\partial t} = \begin{bmatrix} -s\sin\theta\left(\frac{\partial\theta}{\partial t}\right) - \left(\frac{\partial v}{\partial t}\right)\sin\theta - v\cos\theta\left(\frac{\partial\theta}{\partial t}\right) \\ s\cos\theta\left(\frac{\partial\theta}{\partial t}\right) + \left(\frac{\partial v}{\partial t}\right)\cos\theta - v\sin\theta\left(\frac{\partial\theta}{\partial t}\right) \end{bmatrix} \tag{A.3}$$

Consequently, Eq. (A.2) can be further expanded using Eq. (A.3)

$$T_{\mathrm{L}} = \frac{\rho L}{2}\int_0^1 \left\{\left(\frac{\mathrm{d}\theta}{\mathrm{d}t}\right)^2[(\zeta L)^2 + v^2] + 2\zeta L\left(\frac{\mathrm{d}\theta}{\mathrm{d}t}\right)\left(\frac{\partial v}{\partial t}\right) + \left(\frac{\partial v}{\partial t}\right)^2\right\}\mathrm{d}\zeta\,, \tag{A.4}$$

with $s = \zeta L, \zeta \in [0,1]$. Therefore, the variation of T_{L} is calculated as

$$\delta T_{\mathrm{L}} = \rho L\int_0^1 \left\{\left[(\zeta^2 L^2 + v^2)\left(\frac{\mathrm{d}^2\theta}{\mathrm{d}t^2}\right) + v\left(\frac{\mathrm{d}\theta}{\mathrm{d}t}\right)\left(\frac{\partial v}{\partial t}\right) + \zeta L\left(\frac{\partial^2 v}{\partial t^2}\right)\right]\delta\theta + \left[\zeta L\left(\frac{\mathrm{d}^2\theta}{\mathrm{d}t^2}\right) + v\left(\frac{\mathrm{d}\theta}{\mathrm{d}t}\right)^2 + \left(\frac{\partial^2 v}{\partial t^2}\right)\right]\delta v\right\}d\zeta\,, \tag{A.5}$$

Similarly, the kinetic energy of the tip mass is expressed as follows

$$T_{\mathrm{P}} = \frac{m_{\mathrm{p}}}{2}\left(\frac{\partial \boldsymbol{r}_{\mathrm{fl}}}{\partial t}\Big|_{s=L}\right)^{\mathrm{T}}\left(\frac{\partial \boldsymbol{r}_{\mathrm{fl}}}{\partial t}\Big|_{s=L}\right) + \frac{J_{\mathrm{p}}}{2}\left(\frac{\mathrm{d}\theta}{\mathrm{d}t} + \frac{\partial^2 v}{\partial s\partial t}\Big|_{s=L}\right)^2\,, \tag{A.6}$$

where the subscript P denotes the tip mass. Thus, the variation of T_{P} is calculated as

$$\delta T_{\mathrm{P}} = m_{\mathrm{p}}\left[(L^2 + v^2|_{s=L})\left(\frac{\mathrm{d}^2\theta}{\mathrm{d}t^2}\right) + v|_{s=L}\left(\frac{\partial v}{\partial t}\right)\Big|_{s=L}\left(\frac{\mathrm{d}\theta}{\mathrm{d}t}\right)\right]\delta\theta + m_{\mathrm{p}}\left[\left(\frac{\partial v}{\partial t}\right)\Big|_{s=L} + L\left(\frac{\mathrm{d}\theta}{\mathrm{d}t}\right)\right]\delta\left(\frac{\partial v}{\partial t}\right)\Big|_{s=L} + m_{\mathrm{p}}L\left(\frac{\mathrm{d}^2\theta}{\mathrm{d}t^2}\right)\delta v|_{s=L}$$
$$+ J_{\mathrm{p}}\left(\frac{\mathrm{d}^2\theta}{\mathrm{d}t^2} + \frac{\partial^3 v}{\partial s\partial t^2}\Big|_{s=L}\right)\left[\delta\theta + \delta\left(\frac{\partial v}{\partial s}\right)\Big|_{s=L}\right]. \tag{A.7}$$

By combination, Eq. (A.7) can be simplified to

$$\delta T_{\mathrm{P}} = \left\{ m_{\mathrm{p}} \left[\left(L^2 + v^2|_{s=L} \right) \left(\frac{\mathrm{d}^2\theta}{\mathrm{d}t^2} \right) + v|_{s=L} \left(\frac{\partial v}{\partial t} \right) \Big|_{s=L} \left(\frac{\mathrm{d}\theta}{\mathrm{d}t} \right) \right] + J_{\mathrm{p}} \left(\frac{\mathrm{d}^2\theta}{\mathrm{d}t^2} + \frac{\partial^3 v}{\partial s \partial t^2} \Big|_{s=L} \right) \right\} \delta\theta$$

$$+ \left\{ m_{\mathrm{p}} \left[\left(\frac{\partial v}{\partial t} \right) \Big|_{s=L} + L \left(\frac{\mathrm{d}\theta}{\mathrm{d}t} \right) \right] + J_{\mathrm{p}} \left(\frac{\mathrm{d}^2\theta}{\mathrm{d}t^2} + \frac{\partial^3 v}{\partial s \partial t^2} \Big|_{s=L} \right) \right\} \delta \left(\frac{\partial v}{\partial s} \right) \Big|_{s=L} + m_{\mathrm{p}} L \left(\frac{\mathrm{d}^2\theta}{\mathrm{d}t^2} \right) \delta v|_{s=L}. \tag{A.8}$$

In addition, the variation of the kinetic energy from the rotational motor is $\delta T_{\mathrm{m}} = J_{\mathrm{m}} \left(\frac{d^2\theta}{dt^2} \right) \delta\theta$ and the variation of the motor torque virtual work is $\delta W = \tau \delta\theta$. Using Eqs. (A.5) and (A.8) together with Eqs. (10) and (11), the dynamical model described in the expression of Eq. (12) is deduced with Eq. (8) for four variations $\left\{ \delta\theta, \delta v, \delta v|_{s=L}, \delta \left(\frac{\partial v}{\partial s} \right) \Big|_{s=L} \right\}$.

Appendix B

When the axial compression force is selected as the critical buckling load, the value of the lateral stiffness expression Eq. (34) is equal to zero, i.e.,

$$\frac{-F\beta\cos(\beta L)}{-(\beta L)\cos(\beta L) + \sin(\beta L)} + 2k\lambda = 0, \tag{B.1}$$

which is equivalent to

$$-F\beta\cos(\beta L) + 2k\lambda[\sin(\beta L) - (\beta L)\cos(\beta L)] = 0. \tag{B.2}$$

By moving the term $2k\lambda\sin(\beta L)$ to the right hand side of the equation, one obtains

$$F\beta\cos(\beta L) + 2k\lambda(\beta L)\cos(\beta L) = 2k\lambda\sin(\beta L). \tag{B.3}$$

If $\sin(\beta L) \neq 0$, then Eq. (B.3) leads to Eq. (28).

References

1. K. Wu, G. Zheng, G. Hao, Efficient spatial compliance analysis of general initially curved beams for mechanism synthesis and optimization, *Mechanism and Machine Theory* 162 (2021) 104343-1-22.

2. Y. Song, W. He, X. He, Z. Han, Vibration control of a high-rise building structure: theory and experiment, *IEEE/CAA Journal of Automatica Sinica*, 8 (4) (2021) 866-875.

3. W. He, T. Wang, X. He, L. Yang, O. Kaynak, Dynamical modelling and boundary vibration control of a rigid-flexible wing system, *IEEE/ASME Transactions on Mechatronics*, 25 (6) (2020) 2711-2721.

4. B. Kim, T. Park, Estimation of cable tension force using the frequency-based system identification method, *J. Sound Vib.* 304 (2007) 660-676.

5. R. Geier, G. Roeck, R. Flesch, Accurate cable force determination using ambient vibration measurements, *Structure and Infrastructure Engineering* 2 (1) (2006) 43-52.

6. N. Tullini, F. Laudiero, Dynamic identification of beam axial loads using one flexural mode shape, *J. Sound Vib.* 318 (2008) 131-147.

7. B. Yan, W. Chen, J. Yu, X. Jiang, Mode shape-aided tension force estimation of cable with arbitrary boundary conditions, *J. Sound Vib.* 440 (2019) 315-331.

8. L. Ma, A highly precise frequency-based method for estimating the tension of an inclined cable with unknown boundary conditions, *J. Sound Vib.* 409 (2017) 65-80.

9. S. Li, E. Reynders, K. Maes, G. Roeck, Vibration-based estimation of axial force for a beam member with uncertain boundary conditions, *J. Sound Vib.* 332 (2013) 795-806.

10. M. Amabili, S. Carra, L. Collini, et al., Estimation of tensile force in tie-rods using a frequency-based identification method, *J. Sound Vib.* 329 (2010) 2057-2067.

11. L. Ma, H. Xu, T. Munkhbaatar, S. Li, An accurate frequency-based method for identifying cable tension while considering environmental temperature variation, *J. Sound Vib.* 490 (2021) 115693-1-16.

12. T. Kernicky, M. Whelan, E. Al-Shaer, Dynamic identification of axial force and boundary restraints in tie rods and cables with uncertainty quantification using set inversion via interval analysis, *J. Sound Vib.* 423 (2018) 401-420.

13. L. Tang, M. Gouttefarde, H. Sun, et al., Dynamic modelling and vibration suppression of a single-link flexible manipulator with two cables, *Mechanism and Machine Theory* 162 (2021) 104347-1-17.

14. P. Asdaque, S. Banerjee, S. Roy, An electromechanically coupled intrinsic, mixed variational formulation for geometrically nonlinear smart composite beam, *Applied Mathematical Modelling* 65 (2019) 549-565.

15. W. Yu, M. Blair, GEBT: A general-purpose nonlinear analysis tool for composite beams, *Composite Structures* 94 (2012) 2677-2689.

16. D. Hodges, A mixed variational formulation based on exact intrinsic equations for dynamics of moving beams, *International Journal of Solids and Structures* 26 (11) (1990) 1253-1273.

17. H. Sun, X. Tang, Z. Cui, et al., Dynamic response of spatial flexible structures subjected to controllable force based on cable-driven parallel robots, *IEEE/ASME Trans. Mechatron.* 25 (6) (2020) 2801–2811.

18. R. Dixit, R.P. Kumar, Cable stiffened flexible link manipulator, in: *2013 IEEE/RSJ International Conference on Intelligent Robots and Systems (IROS)*, Chicago, USA, 2014, pp. 871–876.

19. H. Yuan, E. Courteille, M. Gouttefarde, et al., Vibration analysis of cable-driven parallel robots based on the dynamic stiffness matrix method, *J. Sound Vib.* 394 (2017) 527-544.

20. J. Kim, S.P. Chang, Dynamic stiffness matrix of an inclined cable, *Eng. Struct.* 23 (12) (2001) 1614–1621.

21. I. Chawla, P. M. Pathak, L. Notash, et al., Effect of Effect of selection criterion on the kineto-static solution of a redundant cable-driven parallel robot considering cable mass and elasticity, *Mechanism and Machine Theory* 156 (2021) 104175-1-23.

22. J. Wei, D. Cao, L. Liu and W. Huang. Global mode method for dynamic modeling of a flexible-link flexible-joint manipulator with tip mass, *Applied Mathematical Modelling* 48 (2017) 787-805.

23. L. Wang, X. Zhang, S. Huang, et al., Measured frequency for the estimation of cable force by vibration method, *J. Eng. Mech.* 141 (2) (2015) 243–253.

24. V. Gattulli, M. Lepidi, Localization and veering in the dynamics of cable-stayed bridges, *Computers & Structures* 85 (2007) 1661-1678.

25. X. He, W. He, J. Shi, C. Sun, Boundary vibration control of variable length crane systems in two-dimensional space with output constraints, *IEEE/ASME Transactions on Mechatronics*, 22 (5) (2017) 1952-1962.

26. L. Caracoglia, D. Zuo, Effectiveness of cable networks of various configurations in suppressing stay-cable vibration, *Engineering Structures* 31 (2009) 2851-2864.

27. G. Giaccu, L. Caracoglia and B. Barbiellini, Modeling "unilateral" response in the cross-ties of a cable network: Deterministic vibration, *J. Sound Vib.* 333 (2014) 4427-4443.

28. G. Giaccu, L. Caracoglia, Generalized pow-law stiffness model for nonlinear dynamics of in-plane cable networks, *J. Sound Vib.* 332 (2013) 1961-1981.

29. D. Zuo, N. Jones and J. Main, Field observation of vertex-and rain-wind-induced stay-cable vibrations in a three-dimensional environment, *Journal of Wind Engineering and Industrial Aerodynamics* 96 (3) (2008) 308-326.

30. Z. Bazant, Structural stability, *Int. J. Solids Struct* 37 (2000) 55-67.

31. C. Wang, C. Wang, J. Reddy, Exact solutions for buckling of structural members, CRC Press, Boca Raton, FL, USA, 2005.

32. H. Debski, T. Kubiak, A. Teter, Buckling and postbuckling behaviour of thin-walled composite channel section column, *Composite Structures* 100 (2013) 195-204.

33. B. Blostotsky, E. Efraim, Y. Ribakov, Improving the reliability of measuring critical buckling load in sway mode frames, *Experimental Mechanics* 56 (2016) 311-321.

34. G. Boscato, S. Ientile, Experimental and numerical investigation on dynamic properties of thin-walled GFRP buckled columns, *Composite Structures* 189 (2018) 273-285.

35. C. Go, Y. Lin, E. Khor, Experimental determination of the buckling load of a straight structural member by using dynamic parameters, *J. Sound Vib.* 205 (3) (1997) 257-264.

36. M. Bilgehan, Comparison of ANFIS and NN models-With a study in critical buckling load estimation, *Applied Soft Computing* 11 (2011) 3779-3791.

37. S. Fan, D. Zheng, Stability of a cracked Timoshenko beam-column by modified Fourier series, *J. Sound Vib.* 264 (2003) 475-484.

38. P. Jiki, Buckling analysis of pre-cracked beam-columns by Liapunov's second method, *Eur. J. Mech. A: Solid* 26 (2007) 503-518.

39. D. Subedi, I. Tyapin, G. Hovland, Dynamic modeling of planar multi-link flexible manipulators, *Robotics* 10 (70) (2021) 1-26.

40. M. Porez, F. Boyer, A. Belkhiri, A hybrid dynamic model for bio-inspired soft robots: application to a flapping-wing micro air vehicle, *Int. Conf. Robot. Autom.* (2014) 3556–3563.

41. D. Lau, D. Oetomo, S. Halgamuge, Inverse dynamics of multilink cable-driven manipulators with the consideration of joint interaction forces and moments, *IEEE Transactions on Robotics* 31 (2) (2015) 478-488.

42. M. Bottin, M. Ceccarelli, C. Morales-Cruz, G. Rosati, Design and Operation Improvements for CADEL Cable-Driven Elbow Assisting Device, *Mechanisms and Machine Science* 91 (2021) 503-511.

43. L. Tang, P. Shi, Design and analysis of a gait rehabilitation cable robot with pairwise cable arrangement, *Journal of Mechanical Science and Technology* 35 (2021) 3161-3170.

44. S. Abdolshah, D. Zanotto, G. Rosati, S.K. Agrawal, Optimizing stiffness and dexterity of planar adaptive cable-driven parallel robots, *Journal of Mechanisms and Robotics* 9 (3) (2017) 031004.

45. P. Shi, L. Tang, Dimensional synthesis of a gait rehabilitation cable-suspended robot on minimum 2-norm tensions, *Journal of Mechanics in Medicine and Biology* 21 (6) (2021) 1–21.

46. S. Seriani, M. Seriani, P. Gallina, Workspace optimization for a planar cable-suspended direct-driven robot, *Robotics and Computer-Integrated Manufacturing* 34 (2015) 1-7.

47. S. Sinir, M. Çevik, B. G. Sinir, Nonlinear free and forced vibration analyses of axially functionally graded Euler-Bernoulli beams with non-uniform cross-section, *Composites Part B* 148 (2018) 123-131.

48. S. Lee, C. Mote, A generalized treatment of the energetics of translating continua, part II: beams and fluid conveying pipes, *J. Sound Vib.* 204 (5) (1997) 735-753.

49. Y. Tang, L. Chen, X. Yang, Natural frequencies, modes and critical speeds of axially moving Timoshenko beams with different boundary conditions, *International Journal of Mechanical Sciences* 50 (2008) 1448-1458.

50. H. Irvine, Cable structures, Massachusetts Institute of Technology (MIT), Cambridge, MA.

51. P. Warnitchar, Y. Fujino, T. Susumpow, A non-linear dynamic model for cables and its application to a cable-structure system, *J. Sound Vib.* 187 (4) (1995) 695-712.

52. F. Driscoll, R. Lueck, M. Nahon, Development and validation of a lumped-mass dynamics model of a deep-sea ROV system, *Applied Ocean Research* 22 (2000) 169-182.

53. J. Merlet, Some properties of the Irvine cable model and their use for the kinematic analysis of cable-driven parallel robots, *Mechanism and Machine Theory* 135 (2019) 271-280.

54. B. Buckham, F. Driscoll, M. Nahon, Development of a finite element cable model for use in low-tension dynamics simulation, *Journal of Applied Mechanics* 71 (2004) 476-485.

55. Y. Liu, L. Xu, Storey-based stability analysis of multi-storey unbraced frames, *Structural Engineering and Mechanics* 2005 (19) (6) 679-705.

56. L. Xu, X. Wang, Stability of multi-storey unbraced steel frames subjected to variable loading, *Journal of Constructional Steel Research* 63 (2007) 1506-1514.

57. L. Chen, Y. Yu, J. Cheng, et al. Accurate analytical approximation to post-buckling of column with Ramberg-Osgood constitutive law, *Applied Mathematical Modelling* 98(2021) 121-133.